GEOLOGICA CARPATHICA, OCTOBER 2018, 69, 5, 483–497 doi: 10.1515/geoca-2018-0028

Accessory minerals and evolution of tin-bearing S-type granites in the western segment of the Gemeric Unit (Western Carpathians)

IGOR BROSKA✉ and MICHAL KUBIŠ

Earth Science Institute of the Slovak Academy of Sciences, Dúbravská cesta 9, 840 05 Bratislava; ✉igor.broska@savba.sk

(Manuscript received May 27, 2018; accepted in revised form October 4, 2018)

Abstract: The S-type accessory mineral assemblage of zircon, monazite-(Ce), fluorapatite and tourmaline in the cupolas of Permian granites of the Gemeric Unit underwent compositional changes and increased variability and volume due to intensive volatile flux. The extended S-type accessory mineral assemblage in the apical parts of the granite resulted in the formation of rare-metal granites from in-situ differentiation and includes abundant tourmaline, zircon, fluorapatite, monazite-(Ce), Nb–Ta–W minerals (Nb–Ta rutile, ferrocolumbite, manganocolumbite, ixiolite, Nb–Ta ferberite, hübnerite), cassiterite, topaz, molybdenite, arsenopyrite and aluminophosphates. The rare-metal granites from cupolas in the western segment of the Gemeric Unit represent the topaz–zinnwaldite granites, albitites and greisens. Zircon in these evolved rare-metal Li–F granite cupolas shows a larger xenotime-(Y) component and heterogeneous morphology compared to zircons from deeper porphyritic biotite granites. The zircon Zr/Hf_{wt} ratio in deeper rooted porphyritic granite varies from 29 to 45, where in the differentiated upper granites an increase in Hf content results in a Zr/Hf_{wt} ratio of 5. The cheralite component in monazite from porphyritic granites usually does not exceed 12 mol. %, however, highly evolved upper rare-metal granites have monazites with 14 to 20 mol. % and sometimes >40 mol. % of cheralite. In granite cupolas, pure secondary fluorapatite is generated by exsolution of P from P-rich alkali feldspar and high P and F contents may stabilize aluminophosphates. The biotite granites contain scattered schorlitic tourmaline, while textural late-magmatic tourmaline is more alkali deficient with lower Ca content. The differentiated granites contain also nodular and dendritic tourmaline aggregations. The product of crystallization of volatile-enriched granite cupolas are not only variable in their accessory mineral assemblage that captures high field strength elements, but also in numerous veins in country rocks that often contain cassiterite and tourmaline. Volatile flux is documented by the tetrad effect via patterns of chondrite normalized REEs (T1,3 value 1.46). In situ differentiation and tectonic activity caused multiple intrusive events of fluid-rich magmas rich in incompatible elements, resulting in the formation of rare-metal phases in granite roofs. The emplacement of volatile-enriched magmas into upper crustal conditions was followed by deeper rooted porphyritic magma portion undergoing second boiling and re-melting to form porphyritic granite or granite-porphyry during its ascent.

Keywords: S-type granite, zircon, fluorapatite, monazite, tourmaline, cassiterite, rare-metal granites, Gemeric Unit.

Introduction

The presence of boron in felsic melt significantly changes the rheological character in density and viscosity (Dingwell et al. 1996), and decreases the solidus temperature (Manning 1981; Pichavant 1981; Pollard et al. 1987). Effective melt depolymerization by boron and fluorine resulted in melt mobility and differentiation, which enables the concentration of lithophile elements, such as Rb, Li, Sn, Nb, Ta (Dingwell et al. 1985). F-rich source magma became more enriched in incompatible elements with increase of heavy rare earth elements (O'Neill et al. 2017). The high volatile flux is an important phenomenon with regard to easier differentiation, emplacement of melt to the shallow crustal level, formation of various rare-metal accessory mineral phases and increase in the metallogenetic capacity. But the behaviour of the high field strength elements is also strongly controlled by the ASI (molar Al/Na+K) parameter (Aseri et al. 2015).

This study presents the characterization of the accessory mineral assemblage in the volatile-rich granite system of Permian granites in the Gemeric Unit (uppermost Alpine tectonic nappe unit of the Western Carpathians). These granites crop out as small bodies in Lower Paleozoic low-grade metavolcano–sedimetary rocks and, according to geophysical data, represent cupolas of a large hidden granite massif with a thickness of ~5 km (Šefara et al. 2017). The Alpine Gemeric Unit was stacked onto the Veporic Unit during the Cretaceous, probably wedging the Hronic Unit in between (e.g., Vozár et al. 2015; Plašienka 2018). The tourmaline is a more typical accessory phase for the Gemeric granites, with its concentration increasing towards the granite cupolas (Rub et al 1977; Broska et al. 2002; Kubiš & Broska 2005). The apical parts of the Gemeric granites, due to high primary concentration of volatiles, contain various accessory minerals of Sn, Nb, Ta, W, B, F and Li and, therefore, Uher & Broska (1996) classified the Gemeric granites as "specialized S-type granites". The special mineralization in granitic rocks is expressed by the presence of cassiterite, Nb–Ta oxides, wolframite, fluorite (Kamenický & Kamenický 1955; Baran et al. 1970; Malachovský et al. 1983, 2000; Broska et al. 2002, Uher et al.

2001) and other Li minerals (zinnwaldite, protolitionite) along with accessory aluminophosphates such as arrojadite, lacroixite, goyazite, gorceixite and viitaniemiite (Petrík et al. 2011, 2014). Several localities of granites in the Gemeric Unit were previously explored for tin. In general, the accessory Nb–Ta oxides are commonly concentrated in the rare-metal pegmatites (Černý & Ercit 2005; Duran et al. 2016) but pegmatites are absent in the Gemeric Unit. Kubiš & Broska (2010) suggested that the formation of the special mineralization in granites comes from a volatile-rich melt or water-enriched magmas under a carapace of the solidified fine-grained granites.

The goal of this contribution is to present the distribution and character of prominent accessory phases in both deeper seated (barren) and apical granites with a special focus on zircon, monazite, apatite and tourmaline.

Methods

The samples were studied from polished thin sections and polished single grain mounts, separated from heavy mineral concentrates. The isolated accessory minerals were studied by binocular microscope first and then some selected grains were fixed in epoxy, cut and polished. Mineral assemblages, associations and textures were determined by petrographic microscope and electron microprobe CAMECA SX 100 at the Geological Survey of the Slovak Republic and some BSE Hnilec images were taken by the Field Emission Electron Probe Microanalyser (Jeol JXA 8530F) housed at the Earth Science Institute of Slovak Academy of Sciences in Banská Bystrica. Operating conditions for microprobe analysis were 15 kV accelerating voltage and 20 μm beam current with a counting time of 10 seconds. The following natural and synthetic standards were used: wollastonite (Si, Ca), MgO (Mg), Al_2O_3 (Al), albite (Na), fayalite (Fe), rhodonite (Mn), $LiTaO_3$ (Ta), $CaWO_4$ (W), orthoclase (K), apatite (P), NaCl (Cl), TiO_2(Ti), $SrTiO_3$ (Sr), SnO_2 (Sn), barite (Ba), $PbCO_3$ (Pb), $LiNbO_3$ (Nb), UO_2 (U), zircon (Zr) and CaF_2 (F).

Characterization of host granites

The granitic rocks from the profile in the western part of the Gemeric unit shown on Fig. 1 are mainly biotite–muscovite leucogranites and porphyritic granites. The deeper part and apical part of the granite are contrasting in composition. The general composition of granite bodies are characterized by high SiO_2 content, prevalence of K over Na, peraluminousity with an average ASI>1.3, low Ca, Mg, Ba, Sr and REEs. Granites from cupolas are characterized by high Li, Rb, Sn, Nb, Ta, F, B, and P (e.g. Malachovský et al. 1983; Broska et al. 2002; Kubiš & Broska 2010; Petrík et al. 2011). The S-type character according to the classification of Chappell & White (2001) is demonstrated by composition, accessory mineral assemblage

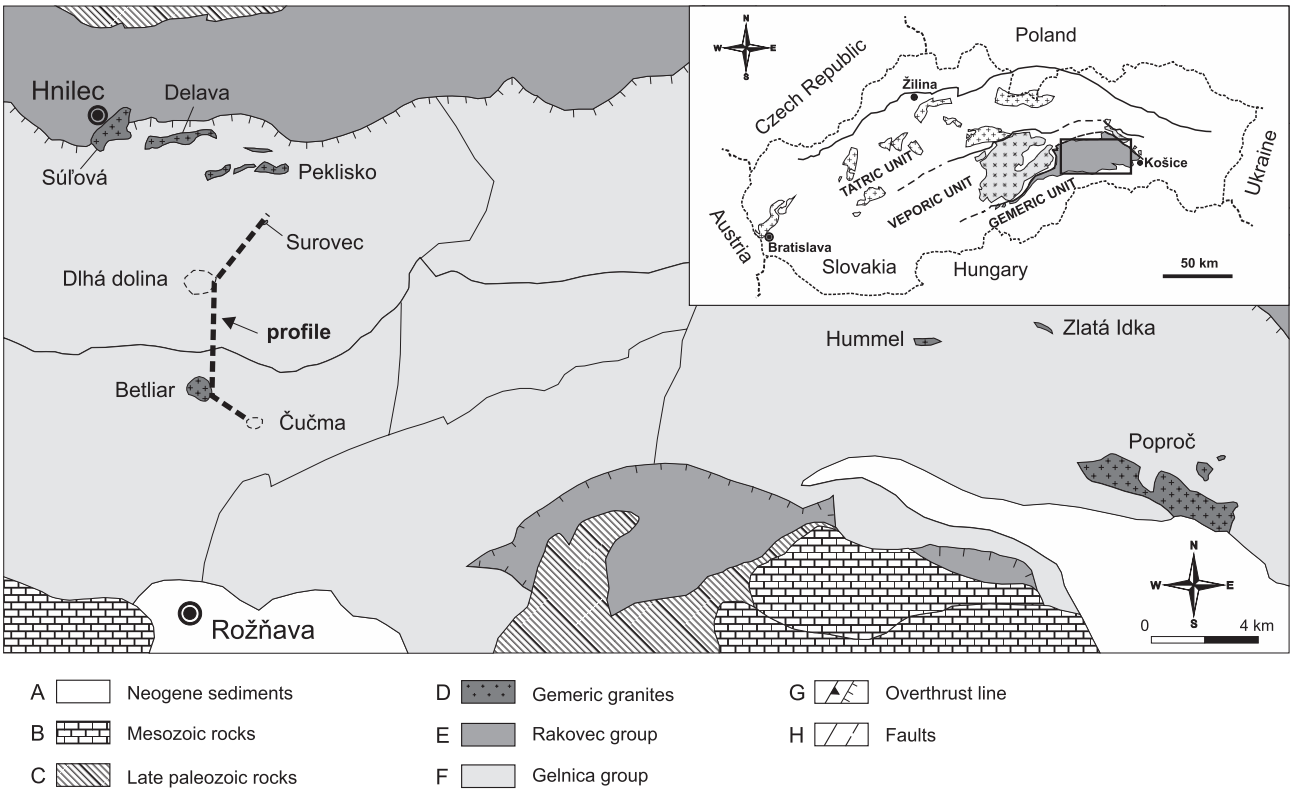

Fig. 1. Geological sketch map showing the position of studied Permian granite bodies along the Surovec–Dlhá Dolina (Podsúľová)–Betliar–Čučma profile which intruded Lower Paleozoic turbidites (modified according to Bajaník et al. 1983).

and a high $^{87}Sr/^{86}Sr$ initial ratio (>0.720 Kovách et al. 1986; Cambel et al. 1990). The high initial Sr isotope ratios, as well as Nd and S isotopic data (Kohút et al. 1999; Kohút & Reccio 2002), indicates a melting of a mature metasedimentary mica-rich feldspathic and pelitic protolith, which resulted in high K, Rb and B contents. Albitization and local greisenization took place in cupolas enriched in volatiles (Dianiška et al. 2002). The highly evolved felsic melt differentiated *in-situ* in cupolas forms tourmaline-bearing Li-biotite granite at the bottom, topaz–zinnwaldite granite in the middle, and quartz-albitite to albitite at the top of the cupola (Breiter et al. 2015).

The porphyritic granites contain more then 1 cm large subhedral crystals of K-feldspar with perthitic structure and large grains of quartz. Strongly sericitized albite with An_{30} cores and biotite flakes with accessory phases correspond to magmatic origin. The fine-grained rare-metal granite contains almost pure albite. All granites contain ubiquitous tourmaline. The upper parts of stocks contain medium-grained protolithionite granite with local K-feldspars up to 1 cm, topaz and accessory Sn–W–Nb–Ta phases are in the matrix. Topaz–zinnwaldite granites are found in cupolas below the albite part with fissures of greisens (Fig. 2a). The uppermost part contains quartz–mica veinlets with some ore phases like Nb–Ta oxides or cassiterite (Fig. 2b).

The Permian ages of these granites were confirmed by dating of monazite (Finger & Broska 1999), MS TIMS method (Poller et al. 2002), SHRIMP geochronology (Radvanec et al. 2009) and LA–ICP–MS (Kubiš & Broska 2010). Kohút and Stein (2005) dated molybdenite in the Hnilec area by Re–Os isotopes and obtained ages of 262±0.9 and 264±0.8 Ma, clearly demonstrating a link between granite evolution and associated metallogenetic processes. SHRIMP dating, indicates the presence of separate granite bodies in the Gemeric Unit because of the time span for their genesis, ~275 Ma for southern Betliar area vs ~258 Ma for the northern Hnilec area (Radvanec et al. 2009; Radvanec & Grecula 2016). Granite bodies are overprinted by Alpine metamorphism making it hard to evaluate their composition (Breiter et al. 2015). The calculated PT conditions of medium-grade Alpine metamorphism reached 600–700 MPa at a temperature of 400 °C (Petrasova et al. 2007). The talc deposit exploited in Gemerská Poloma near Betliar probably originated by fluid activity from the Permian Gemeric granites, which led to the steatitization of carbonate roof rocks and talc formation (Radvanec et al. 2004; see also Grecula et al. 2000).

Results

Characteristics of principal accessory minerals such as zircon, monazite, tourmaline and Sn–W–Nb–Ta-oxides are present in terms of distribution in the two granite settings: (1) porphyritic deep-seated and (2) rare-metal-rich cupolas. The rare-metal granites from cupolas are carriers of economic mineral phases, the deep-seated porphyritic granites are barren and contrast in composition.

Zircon

Zircon morphology according to Pupin's classification (Pupin 1980) typically shows a high amount of S_8 zircon subtypes where pyramid and prismatic faces are equal (see Pupin 1980). Partial zircon edge corrosion is typical, resulting from percolated alkali fluids. Other typical zircon morphological subtypes are S_3, S_4, S_7, S_9 (see also Jakabská & Rozložník 1989). The late magmatic zircon generation consists mainly of metamict crystals with prevalence of G_1 and P_1 subtypes. The less evolved porphyritic granites show higher I.T. values, as in sample GK-6 where I.A.=480 and I.T.=364, but intensively differentiated rare-metal granites show more heterogeneous zircon morphology and often high I.A parameter, as in sample GK-7 where I.A.=524 and I.T.=342 (Fig. 3).

The Zr/Hf_{wt} zircon ratio varies from 29 to 45 in biotite granite, but fractionated granites in cupolas have a typical increase in Hf content towards a smaller Zr/Hf_{wt} ratio, as much as 5. Rims of some zircon grains from highly fractionated Li–F

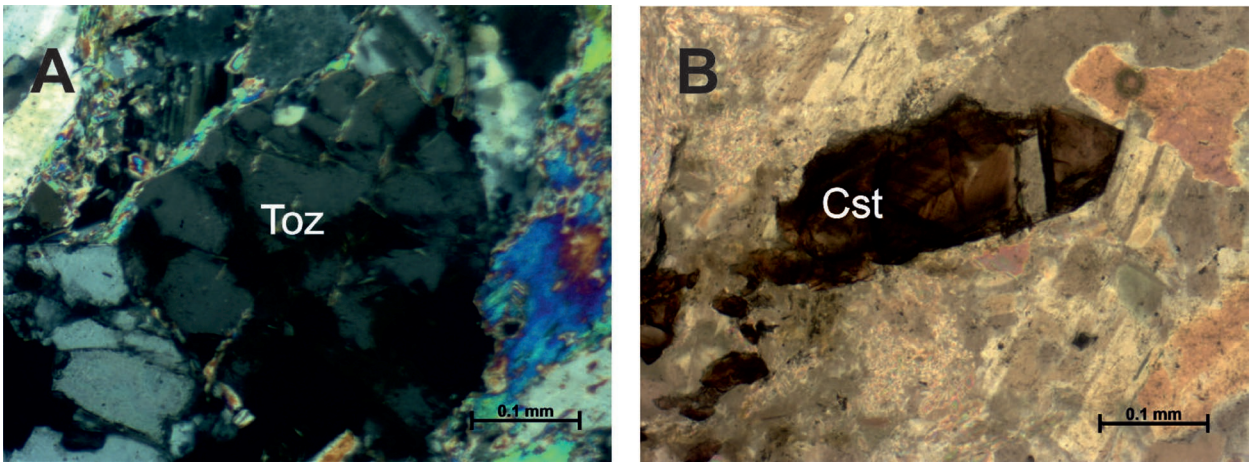

Fig. 2. Microphotos from optical microscope: **A** — topaz and Li-mica in the granite (DD3 570 m); **B** — cassiterite in the greisenized albitite (DD3 489 m).

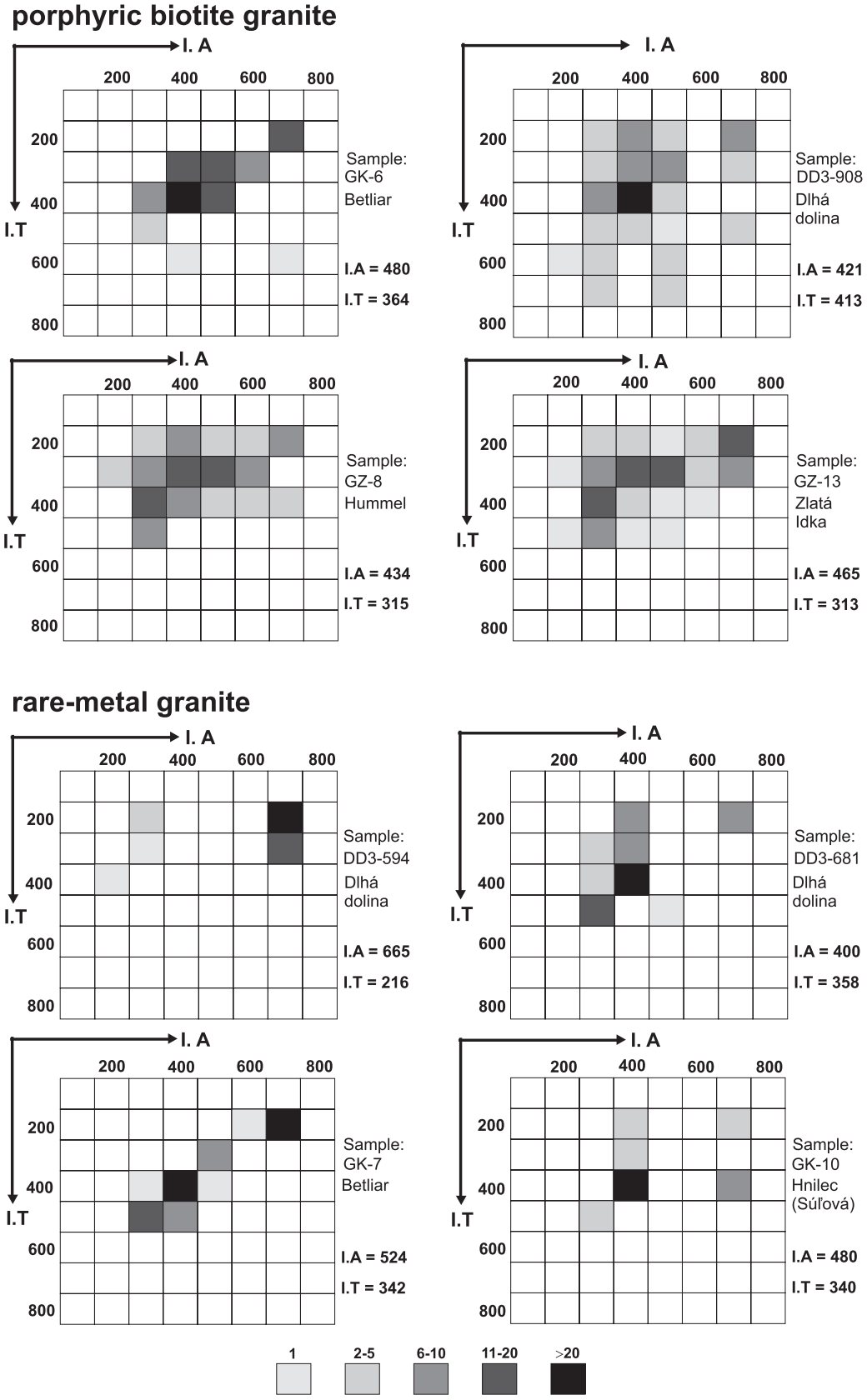

Fig. 3. Representative zircon typological diagrams from specialized S-type granites in the Gemeric Unit. Hummel and Zlatá Idka are the granites form eastern part of the Gemeric Unit, note the differences in zircon morphology from barren deep-seated porphyric biotite granites and apical rare-metal granites.

granites have very high Hf concentrations with more than 9 wt. % HfO_2, increased P content (0.1–2.5 wt. % P_2O_5), up to 2 wt. % UO_2 and 0.9 wt. % Y_2O_3 (Table 1). Substitution mechanisms, except typical $HfZr_{-1}$ substitution, suggests a wide acceptance of the xenotime molecule $(Y,REE)^{3+}P^{5+}Zr^{4+}_{-1}$, Si^{4+}_{-1} (Fig. 4a,b).

Phosphates

Fluorapatite (typically up to 3.5 wt. % Mn) and less monazite and xenotime-(Y) are phosphate phases in deeper-seated barren granites. Fluorapatite may not to be stable enough in the upper rare-metal granites, where low Ca and high F granites stabilize aluminophosphates such as arrojadite, lacroixite, goyazite, gorceixite and viitaniemiite (see Petrík et al. 2011, 2014). Fluorapatite in the upper rare-metal granites precipitated mainly as a secondary, tiny, pure phase exsolved from alkali feldspars (Fig. 5a). In addition Sr-rich fluorapatite is present, from percolated fluids from country rocks, with a rim of the secondary fluorapatite (Fig. 5b). Upper evolved granites concentrate P into feldspars via the berlinite molecule where mainly the rims of alkali feldspars are P-enriched (Fig. 6).

Monazite-(Ce) only exists with enlarged cheralite molecules in the evolved granites. The most important cheralite component in monazite — $CaTh(PO_4)_2$ — from Gemeric granites, usually does not exceed 12 mol. %, however, highly evolved rare-metal granites in the Betliar and Dlhá dolina valley contain monazites with 14 to 20 mol. % and sometimes >40 mol. % of the cheralite molecule (Table 2).

Table 1: Representative zircon analyses from the specialized S-type granites (in wt. %).

Sample	DD3-594/2	DD3-594/7	GK-8A/2	GK-9/1	ZK-31/2-2	ZK-31/1-2
Rock	rare metal granite	rare metal granite	rare metal granite	Ms granite	Ms granite	Ms granite
Locality	Dlhá dolina	Dlhá dolina	Hnilec	Hnilec	Čučma	Čučma
P_2O_5	1.79	0.60	n.a.	n.a.	0.21	0.09
SiO_2	31.65	32.37	33.38	31.12	32.49	32.57
ZrO_2	53.99	58.82	63.71	66.05	65.19	65.07
HfO_2	9.31	6.34	1.83	1.62	1.46	1.01
ThO_2	bdl	0.08	0.01	0.02	bdl	bdl
UO_2	0.69	0.35	0.05	n.a.	bdl	0.04
Y_2O_3	bdl	bdl	0.03	0.21	0.01	bdl
La_2O_3	0.10	bdl	n.a.	n.a.	n.a.	n.a.
Ce_2O_3	0.15	bdl	n.a.	0.02	0.01	0.01
Pr_2O_3	bdl	0.02	n.a.	n.a.	n.a.	n.a.
Nd_2O_3	bdl	0.05	n.a.	n.a.	n.a.	n.a.
Sm_2O_3	0.11	0.05	n.a.	n.a.	0.06	bdl
Er_2O3	0.78	bdl	n.a.	n.a.	0.04	0.04
Yb_2O_3	0.13	0.01	0.04	0.10	0.05	0.02
CaO	0.01	bdl	bdl	bdl	0.03	0.01
Total	98.71	98.69	99.05	99.14	99.55	98.86
Formulae based on 4 oxygen atoms						
P	0.050	0.016	n.a.	n.a.	0.006	0.002
Si	1.005	1.018	1.027	0.974	0.999	1.006
Zr	0.836	0.902	0.956	1.008	0.977	0.980
Hf	0.084	0.057	0.016	0.014	0.013	0.009
Th	bdl	0.001	bdl	bdl	bdl	bdl
U	0.005	0.003	bdl	n.a.	bdl	bdl
Y	bdl	bdl	0.010	0.004	bdl	bdl
La	0.001	bdl	n.a.	n.a.	n.a.	n.a.
Ce	0.002	bdl	n.a.	bdl	bdl	bdl
Pr	bdl	bdl	n.a.	n.a.	n.a.	n.a.
Nd	bdl	0.001	n.a.	n.a.	n.a.	n.a.
Sm	0.001	0.001	n.a.	n.a.	0.001	bdl
Er	0.008	bdl	n.a.	n.a.	0.001	0.001
Yb	0.001	bdl	bdl	0.001	0.001	bdl
Ca	bdl	bdl	bdl	bdl	0.001	bdl
Sum cat.	1.993	1.999	2.001	2.001	1.999	1.998

n.a. — not analysed, bdl — below detection limit

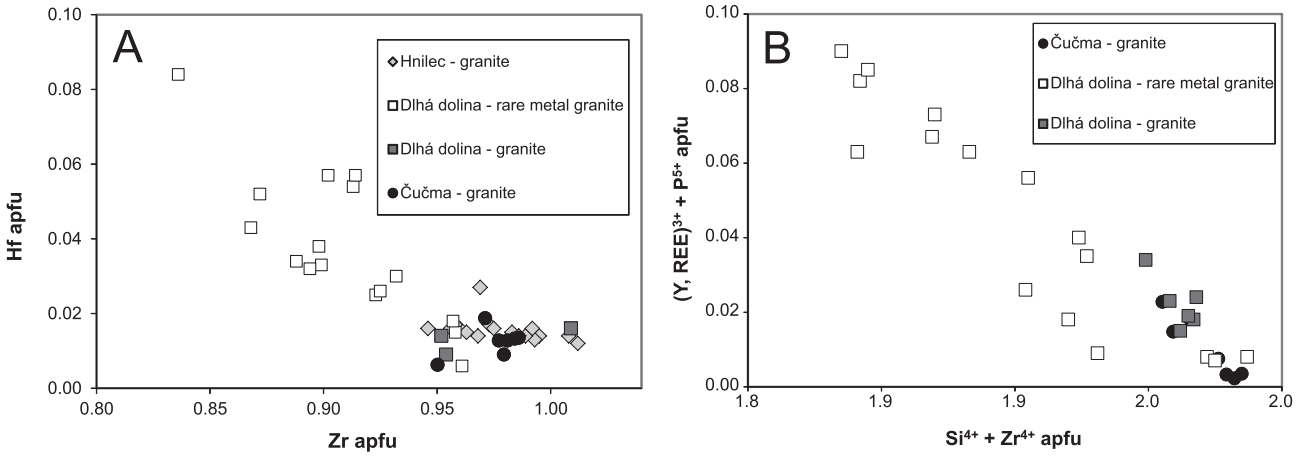

Fig. 4. Substitution diagrams for documented zircon significance: **A** — $HfZr_{-1}$ substitution; **B** — xenotime substitution.

Tourmaline

Representative compositions of tourmalines from all known granite bodies in the Gemeric Unit are presented in Table 3. The tourmaline crystals in granites occur as scattered columnar crystals and 0.x mm aggregates (Fig. 7a). The most evolved granite parts also contain tourmaline nodules, nodules with dendrites on their rims (Fig. 7b) and dendrites. Nodular and dendritic tourmaline is locally common, mainly in the Betliar and Čučma area. Nodular tourmaline is intercalated with alkaline feldspars and quartz, and local light halos forms. Scattered tourmaline from the granites is predominantly schorlitic and alkalic, and typically shows Fe/(Fe+Mg)=0.73 and 0.95, tourmaline in the rare-metal granites commonly have even higher ratios of 0.95 to 1.0 (Fig. 8). The calcium content in tourmaline from the Betliar body decreases from less differentiated to evolved rare-metal equigranular granites.

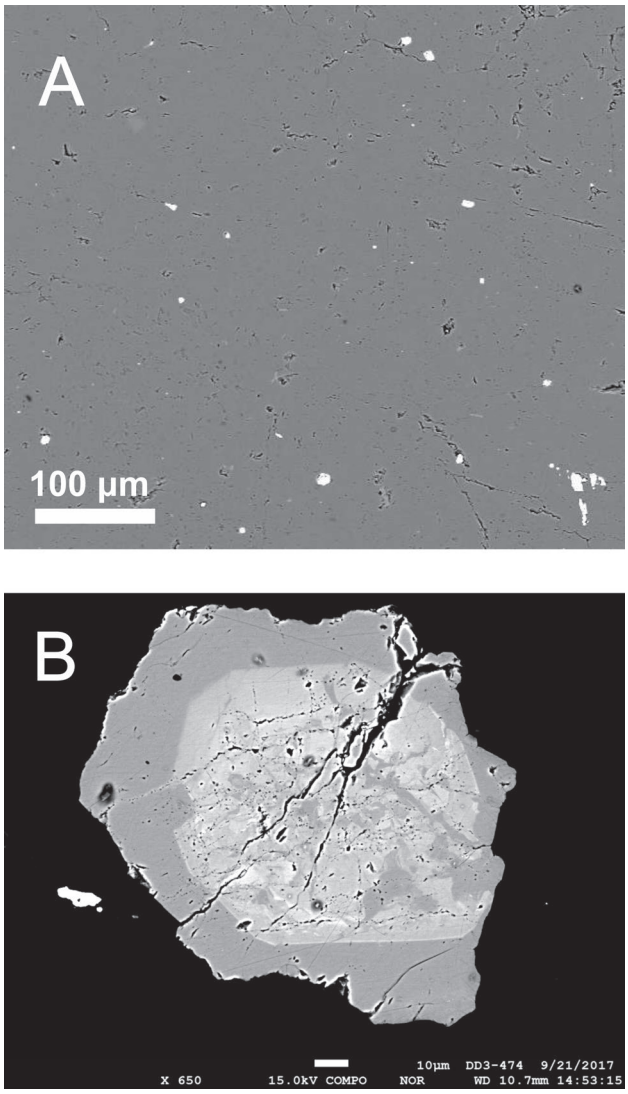

Fig. 5. Backscattered electron image to illustrate P behaviour in the rare-metal granites: **A** — spots represent tiny pure secondary apatites exsolved from the albite; **B** — Sr-rich apatite in veinlets precipitated from vadose fluids contain a secondary generation of pure apatite on rim.

Sn–W–Nb–Ta-oxides

From a metallogenetic point of view, the most common accessory mineral phases in the specialized S-type granites are Sn–W–Nb–Ta-oxides. They are present only in rare-metal granite cupolas or within their altered parts, and in veins emplaced on the hanging wall. Typical evolved granites are topaz- and Li-bearing granites (or zinnwaldite granite) where the accessory mineral paragenesis includes tourmaline (schorlitic to foititic), almandine, topaz, zircon, apatite, monazite-(Ce), xenotime-(Y) and carbonates, but also cassiterite, wolframite, and Nb–Ta oxides (e.g., Malachovský et al. 1983, 2000; Faryad & Dianiška 1989; Broska et al. 1998; Uher et al. 2001). The most important metallogenetic mineral is cassiterite, which occurs mostly in the veinlets of granite apical parts. The granite-related cassiterite-bearing quartz veins and the greisen crop out as a prominent cliff in the upper Dlhá dolina valley.

Ferrocolumbite to manganocolumbite are the most widespread Nb–Ta phases. They often form large euhedral to anhedral, up to 0.3 mm, crystals in association with cassiterite and Nb–Ta rutile. Ferrocolumbite and manganocolumbite often show oscillatory zonality corroded along the margins of crystals with atomic ratios of Mn/(Mn+Fe)=0.18–0.85; Ta/(Ta+Nb)=0.05 and 0.35. Rutile forms 20–60 µm anhedral, strongly zoned crystals in rare-metal granite. It contains up to 9 wt. % Nb_2O_5 and 9–27 wt. % Ta_2O_5; Ta/(Ta+Nb)=0.20–0.76.

Minerals of the wolframite series (ferberite, rarely hübnerite) with Mn/(Mn+Fe)=0.38–0.58 and Ta/(Ta+Nb)=0.04–0.25 occur as platy crystals and fan aggregates, 0.1 mm to 1 cm in size, in rare-metal parts of granites, greisenized parts of albitites and quartz veins (Fig. 9a).

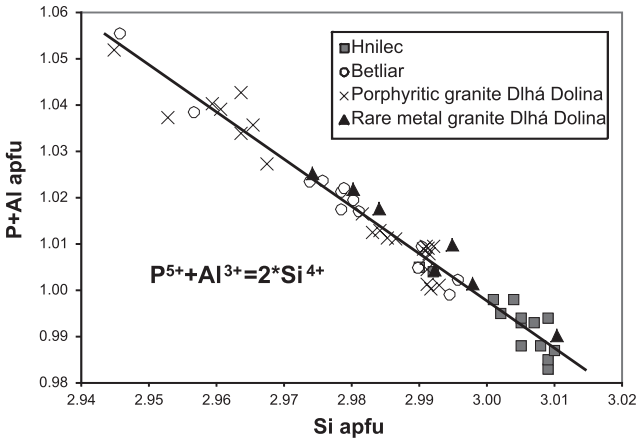

Fig. 6. Berlinite substitution in albite from rare-metal granites. P from berlinite molecule and Ca from anorthite are the main sources for precipitation of secondary apatite. Due to P extraction is its content in feldspars lower in the rare-metal granite.

Table 2: Representative analyses of monazite from the specialized S-type granites (in wt. %).

Sample	GK-6/2	GK-8/14	DD3-808/3-1	DD3-908/3-2	GK7-2-2	GK7-2-9	GK-8/17-1
Rock	Bt granite	Bt granite	Bt granite	Bt granite	rare metal granite	rare metal granite	Ms granite
Locality	Betliar	Hnilec	Dlhá dolina	Dlhá dolina	Betliar	Betliar	Hnilec
Mineral	Mnz	Mnz	Mnz	Mnz	Mnz-Cher	Mnz-Cher	Xtm
SiO_2	0.64	0.55	0.53	0.63	0.51	0.52	0.74
P_2O_5	28.41	29.17	29.37	29.92	27.23	28.51	32.66
CaO	0.55	0.52	2.09	1.10	5.55	5.88	0.13
Y_2O_3	2.23	0.49	3.28	3.62	1.90	2.44	42.19
La_2O_3	12.10	11.03	8.59	10.85	7.11	5.63	bdl
Ce_2O_3	27.23	30.08	22.00	24.60	16.42	14.63	0.15
Pr_2O_3	3.27	3.99	2.35	3.02	1.82	1.78	0.06
Nd_2O_3	12.15	13.28	9.32	10.19	5.85	5.92	0.70
Sm_2O_3	2.76	3.12	2.20	2.12	1.46	1.72	0.94
Eu_2O_3	n.a.	n.a.	0.06	bdl	n.a.	n.a.	n.a.
Gd_2O_3	2.24	1.97	3.51	3.29	2.23	2.40	3.00
Tb_2O_3	n.a.	n.a.	bdl	bdl	0.20	0.20	n.a.
Dy_2O_3	0.88	0.48	1.33	0.59	0.47	0.79	6.85
Ho_2O_3	n.a.	n.a.	0.28	0.61	0.39	0.78	n.a.
Er_2O_3	0.02	bdl	bdl	0.45	0.22	0.11	2.83
Tm_2O_3	n.a.	n.a.	0.34	0.25	n.a.	n.a.	n.a.
Yb_2O_3	0.09	0.07	0.14	0.16	0.07	0.10	1.84
Lu_2O_3	n.a.	n.a.	0.34	bdl	bdl	bdl	n.a.
ThO_2	7.07	4.57	11.54	7.58	25.93	26.19	0.56
UO_2	0.22	0.09	0.69	0.07	2.16	2.78	2.62
Al_2O_3	0.04	0.09	bdl	bdl	bdl	bdl	bdl
TiO_2	n.a.	n.a.	bdl	bdl	n.a.	n.a.	n.a.
MnO	0.06	0.14	0.09	0.05	n.a.	n.a.	0.08
FeO	0.10	bdl	0.40	0.28	n.a.	n.a.	0.12
PbO	bdl	0.01	0.15	0.04	0.37	0.38	0.37
F	bdl	bdl	1.48	0.47	n.a.	n.a.	n.a.
Cl	0.05	0.02	0.04	0.04	n.a.	n.a.	n.a.
Total	100.09	99.67	99.49	99.72	99.89	100.76	95.85
Formulae based on 4 oxygen atoms							
Si	0.102	0.087	0.082	0.097	0.083	0.082	0.026
P	3.837	3.914	3.839	3.915	3.742	3.816	0.970
Ca	0.095	0.089	0.346	0.182	0.965	0.996	0.005
Y	0.189	0.041	0.270	0.298	0.164	0.205	0.787
La	0.712	0.645	0.489	0.619	0.426	0.328	bdl
Ce	1.590	1.745	1.244	1.392	0.976	0.847	0.002
Pr	0.190	0.231	0.132	0.170	0.108	0.103	0.001
Nd	0.692	0.752	0.514	0.562	0.339	0.334	0.009
Sm	0.152	0.170	0.117	0.113	0.082	0.094	0.011
Eu	n.a.	n.a.	0.003	bdl	n.a.	n.a.	n.a.
Gd	0.119	0.104	0.180	0.169	0.120	0.126	0.035
Tb	n.a.	n.a.	bdl	bdl	0.011	0.010	n.a.
Dy	0.045	0.024	0.066	0.029	0.025	0.040	0.077
Ho	n.a.	n.a.	0.014	0.030	0.020	0.039	n.a.
Er	0.001	bdl	bdl	0.022	0.011	0.005	0.033
Tm	n.a.	n.a.	0.016	0.012	n.a.	n.a.	n.a.
Yb	0.004	0.004	0.007	0.008	0.003	0.005	0.020
Lu	n.a.	n.a.	0.016	bdl	bdl	bdl	n.a.
Th	0.257	0.165	0.405	0.267	0.958	0.942	0.004
U	0.008	0.003	0.024	0.002	0.078	0.098	0.020
Al	0.015	0.039	bdl	bdl	bdl	bdl	bdl
Ti	n.a.	n.a.	bdl	bdl	n.a.	n.a.	n.a.
Mn	0.007	0.015	0.010	0.005	n.a.	n.a.	0.002
Fe	0.014	bdl	0.052	0.036	n.a.	n.a.	0.003
Pb	bdl	0.001	0.006	0.002	0.016	0.016	0.004
F	bdl	bdl	0.723	0.230	n.a.	n.a.	n.a.
Cl	0.014	0.005	0.010	0.010	n.a.	n.a.	n.a.
X_{mnz}	91.223	93.633	80.178	88.48	53.48	51.40	
Xbrb	6.273	4.211	17.729	9.03	44.60	46.64	
Xhut	2.505	2.157	2.093	2.49	1.92	1.96	

Cassiterite is the most prominent ore mineral phase in rare-metal granites, greisens and quartz veins in Podsúľová (Dlhá dolina valley) and Betliar, as well as in Hnilec, Zlatá Idka and Poproč. It forms euhedral 0.1–5 mm crystals or aggregates, and veinlets (Fig. 9b). Cassiterite contains up to 1.2 wt. % Nb_2O_5 and 2.2 wt. % Ta_2O_5. Disseminated magmatic cassiterite and Nb–Ta oxides crystallize in the albitic segments of granite cupolas, whereas disseminated wolframite appears mainly in lower topaz-zinnwaldite granite. Cassiterites from the uppermost parts contain a lower amount of minor elements.

High fluid activity is necessary for the effective accumulation of Sn–W–Nb–Ta-oxides into the fluid phase. Mutual compositional relationships in the rare-metal phases are documented by the Nb+Ta−Ti+Sn+W−Fe+Mn multi-cation diagram (Fig. 9); selection of analyses are shown in Table 4. These rare-metal mineral phases can commonly form individual grains several micrometers in size.

Discussion

Interpretation of phosphorus mobility

The fluorapatite evolution is important for understanding the phosphorus behaviour in the evolved granite system. Fluorapatite is developed in three generations: (1) magmatic with high Mn (2) secondary as a pure fluorapatite exsolved from alkalic feldspars and (3) in veinlets from circulated fluids from country rock; the mechanism of P incorporation into alkali feldspars is well known, as well as the phenomenon of its exosolution (London et al. 1990; Breiter et al. 2002, 2017). The absence or low amount of primary apatite at low CaO/P_2O_5 ratios in the granite apical parts and high F activity during late granite crystallization result in a P increase in granite melts and P being incorporated in feldspars. Increasing P is buffered by precipitation of lacroixite and topaz, which become stable at the expense of apatite and albite (Petrík et al. 2011). A probable decrease of pressure during the emplacement of granite along with high fluid activity led to the P exsolution from the alkali feldspars and formation of tiny pure secondary apatites. The secondary apatite exsolved from feldspars by corrosive fluids indicate the general

high P mobility and P penetration towards granite exocontacts.

Števko et al. (2015) described hydrothermal quartz veins hosted by topaz–zinnwaldite leucogranite from the Dlhá dolina area with an association of phosphates and aluminophosphates (fluorapatite, triplite, arrojadite-group minerals and viitaniemiite). Such veins in host rare-metal granites is additional evidence for the intensive mobilization of phosphate from alkali feldspars. Intensive mobilization of the P towards country rocks of evolved granites led to the formation of veins rich in apatite, monazite-(Ce), xenotime-(Y) and U–Th phases in the Čučma ore district. Rojkovič et al. (1999) suggested the host metasediments as element sources for the REE–Th–P rich vein in the nearby Betliar and Čučma granites (Grecula et al. 1995).

Table 3: Selected analyses of tourmaline from the specialized S-type granites from Betliar and Dlhá dolina.

Sample	GK6/4-7	GK6/4-8	GK17/11	GK17/1-3	DD3-908/2
Rock	porphyritic bt granite	porphyritic bt granite	rare-metal ms granite	rare-metal ms granite	rare metal ms granite
Locality	Betliar	Betliar	Betliar	Betliar	Dlhá Dolina
Mineral	schorl	schorl	schorl	schorl	schorl
SiO_2	34.95	34.86	35.34	34.77	35.05
TiO_2	0.80	0.45	0.77	0.40	0.01
B_2O_3*	10.38	10.47	10.44	10.30	10.24
Al_2O_3	33.26	35.19	34.37	34.11	33.93
Cr_2O_3	bdl	bdl	bdl	bdl	0.01
FeO	12.40	11.41	12.93	15.20	13.40
MnO	0.15	0.15	0.15	bdl	0.25
MgO	2.56	2.40	1.15	bdl	0.65
CaO	0.35	0.33	0.16	0.08	0.04
Na_2O	2.12	1.95	1.80	1.98	1.89
K_2O	0.05	0.08	0.03	0.04	0.02
H_2O*	3.38	3.30	3.44	3.55	3.34
F	0.54	0.67	0.35	bdl	0.40
Cl	bdl	bdl	bdl	bdl	0.01
O=F	−0.23	−0.28	−0.15	bdl	−0.17
O=Cl	bdl	bdl	bdl	bdl	bdl
Total	100.30	100.61	100.78	100.43	99.07
Formulae normalised on 31 anions, B=3 and OH+F=4 atoms					
Si^{4+}	5.850	5.786	5.882	5.867	5.947
Al *T*	0.150	0.214	0.118	0.133	0.053
Sum *T*	6.000	6.000	6.000	6.000	6.000
B^{3+}	3.000	3.000	3.000	3.000	3.000
Al *Z*	6.000	6.000	6.000	6.000	6.000
Ti^{4+}	0.101	0.056	0.096	0.051	0.001
Al *Y*	0.411	0.670	0.625	0.651	0.733
Cr^{3+}	bdl	bdl	bdl	bdl	0.001
Fe^{2+}	1.685	1.584	1.800	2.145	1.902
Mn^{2+}	0.021	0.021	0.021	bdl	0.036
Mg^{2+}	0.639	0.505	0.285	bdl	0.164
Sum *Y*	2.857	2.836	2.827	2.847	2.837
Al_{tot}	6.561	6.884	6.743	6.784	6.786
Ca^{2+}	0.063	0.059	0.029	0.014	0.007
Na^{+}	0.688	0.628	0.581	0.648	0.622
K^{+}	0.011	0.017	0.006	0.009	0.004
Sum *X*	0.762	0.704	0.616	0.671	0.633
Vac *X*	0.238	0.296	0.384	0.329	0.367
OH *V*	3.000	3.000	3.000	3.000	3.000
OH_{tot}	3.714	3.648	3.816	4.000	3.782
OH *W*	0.714	0.648	0.816	1.000	0.782
F^{-}	0.286	0.352	0.184	bdl	0.215
Cl^{-}	bdl	bdl	bdl	bdl	0.003
Sum *W*	1.000	1.000	1.000	1.000	1.000
Fe/(Fe+Mg)	0.73	0.76	0.86	1.00	0.92

Interpretation of boron mobility

According to the recent tourmaline supergroup nomenclature (Henry et al. 2011), the tourmaline in the Gemeric granites is predominantly schorlitic and foititic. There is a prevalence of ferrous iron in tourmaline (Broska et al. 1998) indicating mostly reducing conditions during precipitation. The schorlitic tourmaline is more prevalent, but the later generation can be foititic and these may be related to a later stage of influx by low *T* fluids. The multistage formation of tourmaline has been characterized in the Hnilec area by Jiang et al. (2008) and in the Betliar area by Kubiš & Broska (2010). Jiang et al. (2008) described two major generations of the schorlitic–dravitic series: (1) the M (magmatic)-stage which forms zoned tourmaline crystals with the cores enriched in Fe, Al, and Mn, and (2) the L (late)-stage which is more Mg-rich and Fe, Al, Mn depleted. The L-stage occurs in small veins or irregular patches along fractures and cracks and in the contact metapelites. The boron isotopic compositions of the M-stage tourmalines vary from −10.3 ‰ to −15.4 ‰; the L-stage tourmalines have lower $\delta^{11}B$ value of −16.0 ‰ to −17.1 ‰ (Jiang et al. 2008). Kubiš & Broska (2010) recognized four tourmaline types in the Betliar granite body: (1) disseminated magmatic tourmaline, (2) nodular tourmaline formed near solidus temperatures, (3) quartz–schorlitic tourmaline veins, and (4) metamorphic dravitic tourmaline in country rocks connected with B escape from the granites.

The tourmaline composition can be generally typomorphic because it reflects the host rock conditions (Dutrow & Henry 2011; van Hinsberg et al. 2011). The schorlitic chemistry of the primary tourmaline in the granites of the Gemeric Unit is world-wide typical although the dravitic-schorlitic series as in the eastern Pontides are also common (Yavuz et al. 2008). Tourmaline from leucogranites in Zamora (Spain) is schorlitic and dravitic and their rare-metal pegmatites mostly belong to the schorl–elbaite series (Roda-Robles et al. 2004). Tourmaline in the rare-metal granites is schorlitic, commonly nodular and dendritic indicating undercooling and rapid growth. For comparison, tourmalines from the granites in the Poproč areas of the Gemeric Unit are more foititic (Fig. 8).

The formation of nodular tourmaline is related to magmatic crystallization and hydrothermal fluids from penetrated granites (e.g., Samson & Sinclair 1992; Buriánek & Novák 2007). Balen & Broska (2012) interpreted the tourmaline nodules at Moslavačka Gora in Croatia as a result of decompression and ascent of fluids during shallow emplacement of the granite body or formation of vapour and boron-rich-bubbles migrating through the final granite melt. In contrast, Drivenes et al. (2015) suggest formation of larger quartz–tourmaline orbicules

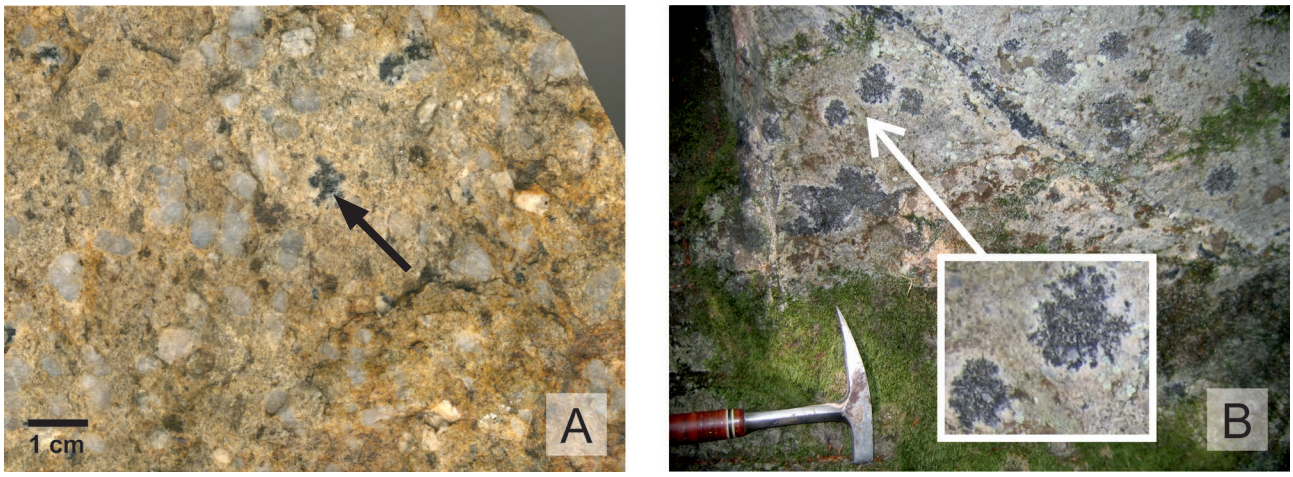

Fig. 7. Tourmaline in the specialized S-type granites from the Betliar area: **A** — scattered grains in porphyritic biotite granite (note fine-grained matrix); **B** — tourmaline nodules from rare-metal granite with a detailed view on the dendritic rims.

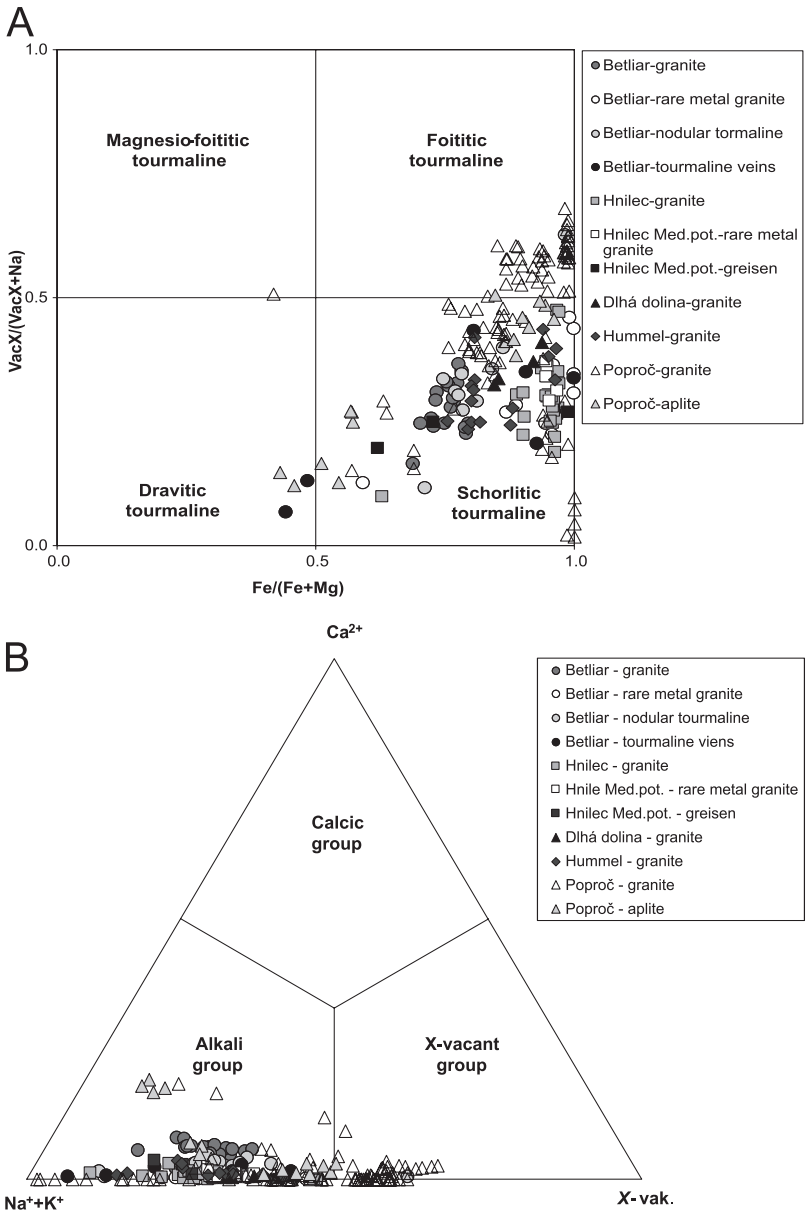

Fig. 8. Classification diagrams of tourmaline according to Henry et al. (2011): **A** — Fe/(Fe+Mg) vs. vacX/(vacX+Na); **B** — Na+K vs X-vac vs Ca. For comparison, the tourmaline compositon from the Poproč and Hummel area (eastern part of the Gemeric Unit) is shown.

in Land's End granite (SW England) from immiscible hydrous borosilicate melts produced during late-stage crystallization. Trumbull et al. (2008) presented a similar evolution, where the tourmaline-rich orbicules were formed late in the crystallization history from an immiscible Na–B–Fe-rich hydrous melt. Flat dendritic tourmaline supports the importance of hydrothermal processes in the evolution of the Gemeric granites, as well as rapid cooling by pressure drop resulting in the escape of fluids of a partly solidified magma (Petrík et al. 2011). On the other hand, according to Perugini & Poli (2007), dendritic tourmaline crystallizes due to limited B diffusion. The decrease in the melting point of boron-rich magma probably led to late tourmaline precipitation of scattered tourmalines in local granite segments, followed by origin of tourmaline nodular dendrites.

Tourmaline precipitation occurs in open systems with bulk contributions from different sources. According to London et al. (1990), tourmaline is particularly abundant in sites with mixing magmatic and wall-rock fluid systems with a tourmaline–biotite antagonism. Therefore, the presence of both biotite and tourmaline in the granite of the Betliar area can be explained by

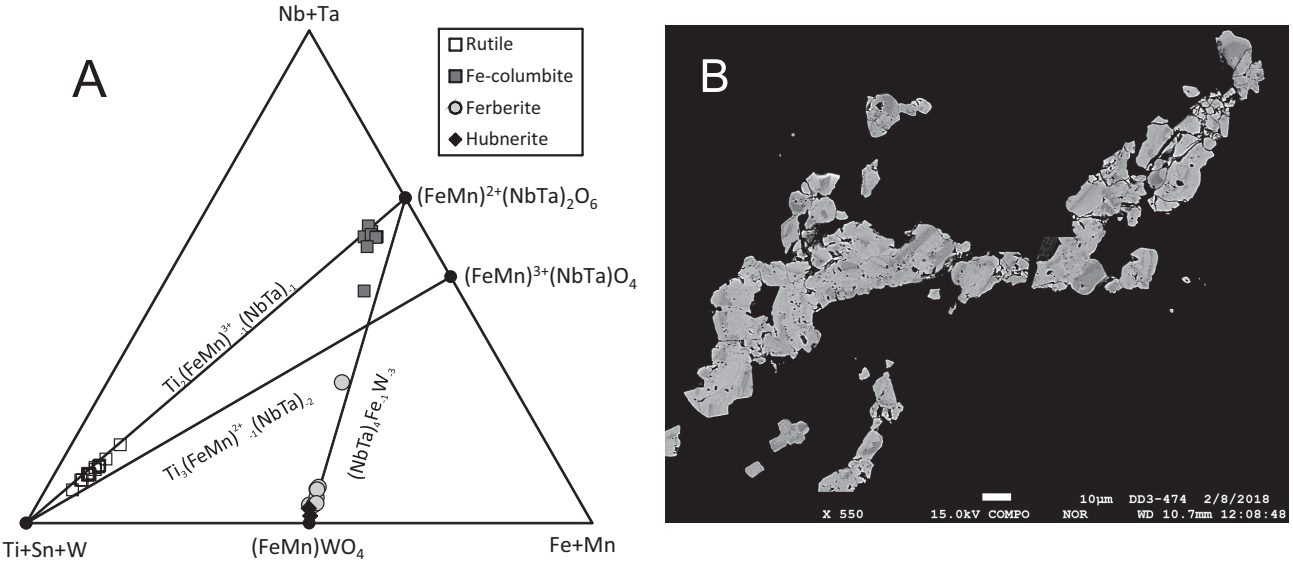

Fig. 9. A — Nb+Ta−Ti+Sn+W−Fe+Mn diagram from accessory mineral phases in the specialized S-type granite (rare-metal type). **B** — BSE of zonal cassiterite from a veinlet in the albitite associated with Nb–Ta oxide (drillcore DD3, depth 474 m).

Table 4: Analyses of Sn, W, Nb, Ta-minerals from rare-metal granites (specialized S-type granites from locality Dlhá dolina).

Sample	**DD3-577/1-4**	**DD3-577/1-6**	**DD3-577/1-10**	**DD3-577/1-11**	**DD3-577/6-6**	**DD3-577/8-1**	**DD3-577/1-13**	**DD3-577/4-2**
Locality	Dlhá dolina	Dlhá dolina	Dlhá dolina	Dlhá dolina	Dlhá dolina	Dlhá dolina	Dlhá dolina	Dlhá dolina
Mineral	Rutile	Rutile	Fe-columb.	Fe-columb.	Ferberite	Ferberite	Hubnerite	Hubnerite
WO_3	bdl	0.26	4.80	2.31	67.78	71.52	72.25	71.34
Nb_2O_5	7.37	6.84	47.60	40.39	5.96	3.08	1.02	2.28
Ta_2O_5	12.52	13.11	23.98	35.06	0.94	0.19	0.44	0.54
TiO_2	73.90	73.18	3.64	4.00	0.32	0.22	0.72	0.70
SnO2	1.23	1.04	1.14	1.83	0.55	0.37	0.19	0.35
ThO_2	bdl	bdl	bdl	bdl	bdl	0.07	bdl	bdl
UO_2	bdl	bdl	bdl	bdl	0.09	0.04	bdl	bdl
Sc_2O_3	bdl	0.04	0.16	0.09	0.16	0.37	0.30	0.57
Sb_2O_3	bdl	bdl	bdl	0.15	0.10	bdl	bdl	bdl
Fe_2O_3	1.62	1.80	bdl	bdl	1.17	1.05	1.57	0.69
FeO	3.22	3.18	14.56	11.97	12.95	13.36	7.85	9.04
MnO	0.04	0.05	3.21	4.66	9.07	8.89	13.85	13.00
ZnO	0.05	bdl	0.12	bdl	bdl	bdl	bdl	bdl
Total	99.95	99.5	99.21	100.46	99.09	99.16	98.19	98.51
Formulae based on 24 oxygens and 12 cations Fe^{3+} and Fe^{2+} calculated by charge-balancing								
W	bdl	0.012	0.313	0.155	5.196	5.543	5.666	5.558
Nb	0.599	0.560	5.413	4.716	0.797	0.416	0.140	0.310
Ta	0.612	0.646	1.640	2.462	0.076	0.015	0.036	0.044
Ti	9.987	9.966	0.689	0.777	0.071	0.049	0.164	0.158
Sn	0.088	0.075	0.114	0.188	0.065	0.044	0.023	0.042
Th	bdl	bdl	bdl	bdl	bdl	0.005	bdl	bdl
U	bdl	bdl	bdl	bdl	0.006	0.003	bdl	bdl
Sc	bdl	0.006	0.035	0.020	0.041	0.096	0.079	0.149
Sb	bdl	bdl	bdl	0.016	0.012	bdl	bdl	bdl
Fe^{3+}	0.219	0.246	bdl	bdl	0.260	0.235	0.358	0.157
Fe^{2+}	0.483	0.481	3.063	2.585	3.203	3.341	1.985	2.272
Mn	0.006	0.008	0.684	1.019	2.273	2.252	3.550	3.310
Zn	0.007	bdl	0.022	bdl	bdl	bdl	bdl	bdl
Total	12.001	12.000	11.973	11 .938	12.000	11 .999	12.001	12.000
Mn/(Mn+Fe)	0.008	0.011	0.183	0.283	0.396	0.386	0.602	0.577
Ta/(Ta+Nb)	0.505	0.536	0.233	0.343	0.087	0.035	0.205	0.124

bdl — below detection limit

the emplacement of granite from a deeper seated magma chamber and contamination by boron, which probably took place during the magma ascent. The fluid influence from country rock is indicated by the presence of Sr-rich apatite (Fig. 5b). The dolomite crystals in granite cupolas are further a product of mixing volatiles from the contact zone with Mg-rich phases (talc, magnesite). Similar Sr mobility from country rock into Sr-poor differentiated granites is known, for example also in the Beauvoir massif (Charoy et al. 2003) and in the San Elias pegmatite from Argentina (Galliski et al. 2012).

Scenario of granite evolution in the Gemeric Unit

The high flux regime in the granite cupolas also demonstrates the tetrad effect on REE's chondrite normalized patterns (Fig. 10). According to Bau (1996) the tetrad effect is formed by the complexation of the REEs with H_2O, CO_2, F^-, and Li^+. The behaviour of the REEs when the tetrad effect occurs is no longer dependent on the ionic radii, but rather on filling stages of 4f orbitals (Irber 1999). Thus, REEs with 0/4 (La), 1/4 (Nd, Pm), 2/4 (Gd), 3/4 (Ho, Er) and 4/4 (Lu) filling 4f orbitals can be fractionated from the other REEs resulting in the tetrad pattern. The tetrad effect occurs in highly evolved igneous rocks as an indicator of the transition between magmatic to high-temperature hydrothermal systems. The separation of F-rich hydrosaline melt in granite cupolas possibly caused the tetrad effect as described Badanina et al. (2006), however, the REE tetrad effect may also develop before magma evolved from a crustal source (Lee et al. 2018).

Due to high volatile flux, the evolution of the specialized S-type granites is different from other Variscan granites in the Western Carpathians. The preserved granite cupolas of larger hidden granite body (Plančár et al. 1977; Šefara et al. 2017), intensive in-situ differentiation and percolation of fluids resulted in formation of various accessory phases in cupolas, including those with metallogenic significance. The tin bearing granite was described in detail by Malachovský et al. (1992); Dianiška et al. (2002); Kubiš & Broska (2010); Breiter et al. (2015) on results from a drilling programme in the Dlhá dolina or Podsúľová area in the Gemeric Unit. The granite outcrops in Betliar and granite emplacement in the Čučma ore district (porphyritic and fine grained granites along mineralized fault — see Grecula et al. 1995) facilitates the proposed scenario for evolution of rare-metal granites as a phase derived from water-rich magma in granite apical part under a carapace of host rock and underlying coarse-grained biotite granites. These composite granite bodies comprise from the bottom (1) a lower coarse-grained barren biotite granite system and (2) mobile apical Li-bearing and topaz–zinnwaldite rare-metal granites associated with greisenized albitites (Fig. 11).

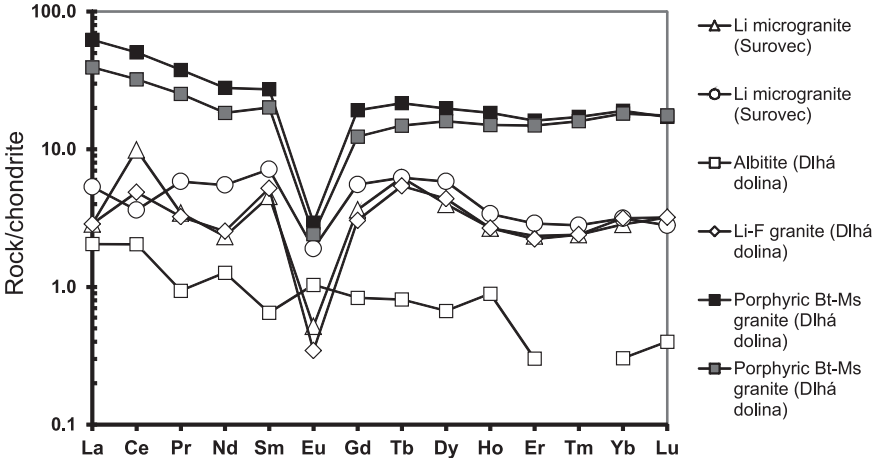

Fig. 10. Tetrad effect in chondrite normalized granites indicates the high flux of volatiles in the rare-metal granite system. The pattern from albitite is for comparison.

Comparison with rare-metal (element) granites

The rare-metal granites belongs to the S- and A-type granites and usually form composite bodies. A-type granite systems are known from Egypt (Gaafar & Ali 2015), and the Erzgebirge (Breiter 2012) or Slavkovský les (Breiter et al. 1999). The S-type rare-metal systems are more widespread, including the Gemer granites (see overview Romer & Kroner 2016). The early Permian S-type Cornubian Batholith is a composite pluton formed from 5 pulses, including granites rich-in-tourmaline (Simons et al. 2017). The western Erzgebirge rare-metal granites show S-type characteristics (e.g., Podlesí), where the eastern part is an A-type (Breiter 2012). The eastern Erzgebirge locality at Cínovec is formed of two different geochemical and mineralogical granites — the rare-metal Sn–W–Nb–Ta–Li-bearing granite intruded after emplacement of deeper seated barren biotite granite and fluid escape from the rare-metal phase causing explosive brecciation of the country rocks (Breter et al. 2017). The rare-metal granites in Cínovec were emplaced into a subvolcanic level (Müller et al. 2005). Breiter et al. (2017) suggested hydrofracturing in the cupola of the rare-metal granite and F and Li partitioning to the fluids, which caused greisenization followed by albitization. The residual melt represents a dry and mica-poor portion. Mineralization in the cupolas of the Gemeric S-type granites is also connected with partitioning of F, Li, and high field strength elements to fluids, although the Cínovec granite is without significant B content. The S-type Gemeric granites reached the upper crustal level, forming a contact aureola of biotite + andaluzite ± cordierite ± corundum at 450–560 °C and P 100–150 MPa (Faryad in Krist et al. 1992), and cannot trigger the brecciation of country rock in such conditions. The comparison of thickness of rare-metal granites in the Gemeric cupolas, which reached less than several hundred m from the surface, with other rare-metal granite systems in the Variscan orogeny in Europe is

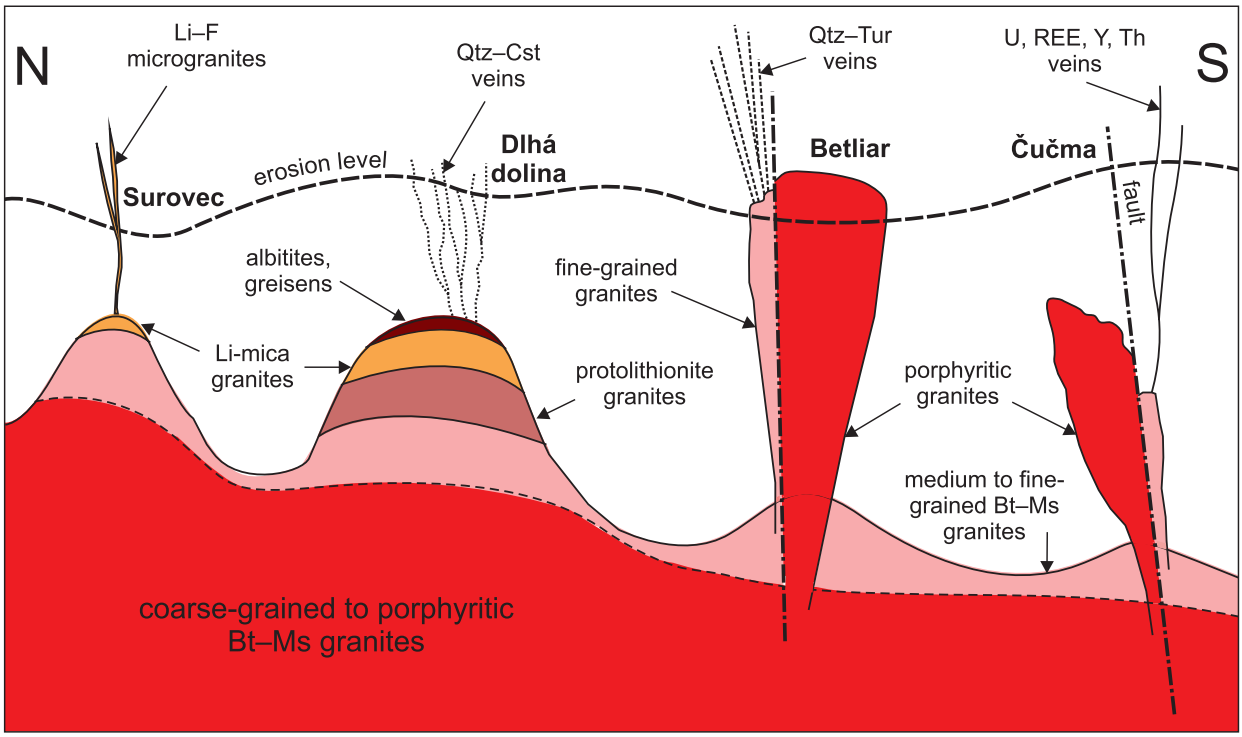

Fig. 11. Idealized cross-section of granite bodies in the profile from Fig. 1 (not to scale) shows a geological evolution prior to superimposed Alpine north vergent thrusting and imbrications (see e.g., Németh 2002; Lexa et al. 2003). The tentative sketch is based on data and interpretation of Dianiška et al. (2002), Kubiš & Broska (2010), Breiter et al. (2015), Pecho et al. (1980) and the geological profile form the Henclová–Surovec area shown by Malachovský (1992) in Grecula et al. (1995).

described in detail by Breiter et al. (2015). Such rare-metal granites are exploited in France, Portugal and Spain as sources of feldspar, columbite–tantalite and cassiterite, but Li separation is still not efficient. The Beauvoir Massif (France) shows disseminated rare-metal mineralization (e.g., Charoy et al. 2003). In general, Nb–Ta mineral phases are recovered from rare-metal granites and granitic rare-element pegmatites (Melcher et al. 2017).

The magmatic evolution of the F-, Li-, B-, H_2O-enriched Kymi topaz granite system is similar in evolution to the granites in the Gemeric Unit. The Kymi zoned stock is a result of intrusion of highly evolved melt from the deeper part of the magma chamber along the fractured contact between the porphyritic granite and the country rock. This evolution was proven by the melt inclusions (Lukkari et al. 2009). The evolution of tin-bearing granites from Eurajoki stock in Finland resulted from similar evolution of F-enriched late-stage peraluminous leucocratic granite (Haapala 1997).

Conclusion

The Permian granites in the Gemeric Unit evolved differentiated cupolas affected by magmatic fluids. This process resulted in the formation of a wider special accessory mineral assemblage that extended former S-type granitic associations. The typical S-type accessory mineral paragenesis in deep-seated barren biotite–muscovite granites contains mainly tourmaline, zircon, apatite, monazite-(Ce), xenotime-(Y), ilmenite, rutile, titanite, thorite, garnet and pyrite. The highly evolved apical rare-metal granites form a more variable accessory assemblage which includes abundant tourmaline, zircon, apatite, monazite-(Ce), Nb–Ta–W minerals (Nb–Ta rutile, ferrocolumbite, manganocolumbite, ixiolite, Nb–Ta ferberite, hübnerite), cassiterite, topaz, molybdenite, arsenopyrite and rare accessory aluminophosphates (arrojadite, lacroixite, goyazite, gorceixite and viitaniemiite).

Acknowledgements: The research was supported by projects APVV 14-0278 and VEGA 2/0084/17. Authors are grateful to Viera Kollárová for measurements using the microprobe at Dionýz Štúr Geological Institute and to Tomáš Mikuš at the Earth Science Institute of the Slovak Academy of Sciences, Banská Bystrica.

References

Aseri A.A., Linnen R.L., Che X.D., Thibault Y. & Holtz F. 2015: Effects of fluorine on the solubilities of Nb, Ta, Zr and Hf minerals in highly fluxed water-saturated haplogranite melts. *Ore Geol. Rev.* 64, 736–746.

Badanina E.V., Trumbull R.B., Dulski P., Wiedenbeck M., Veksler I.V. & Syritso L.F. 2006: The behaviour of rare-earth and lithophile trace elements in rare-metal granites: a study of fluorite, melt inclusions and host rocks from the Khangilay complex, Transbaikalia, Russia. *Can. Mineral.* 44, 667–692.

Bajaník Š., Hanzel V., Ivanička J., Mello J., Pristaš J., Reichwalder P., Snopko L., Vozár J. & Vozárová A 1983: Explanation to geological map 1:50,000 — Slovak Ore Mountains Eastern part. *Dionýz Štúr Inst. Geol. Monogr*., 1–223 (in Slovak with English summary).

Balen D. & Broska I. 2011: Tourmaline nodules: products of devolatilization withon the final evolutionary stage of granite melt? *Geol. Soc. London, Spec. Paper* 350, 53–68.

Baran J., Drnzíková L. & Mandáková K. 1970: Sn–W ore mineralisation related to Hnilec granite. *Mineralia Slovaca* 2, 159–164 (in Slovak).

Bau M. 1996: Controls on the fractionation of isovalent trace elements in magmatic and aqueous systems : evidence fromY/Ho, Zr/Hf, and lanthanide tetrad effect. *Contrib. Mineral. Petrol.*, 123, 323–333.

Breiter K. 2012: Nearly contemporaneous evolution of the A- and S-type fractionated granites in the Krušne Hory/Erzgebirge Mts. Central Europe. *Lithos* 151, 105–121.

Breiter K., Förster H. & Seltmann R. 1999: Variscan silicic magmatism and related tin-tungsten mineralization in the Erzgebirge–Slavkovský les metamollgenic province. *Miner. Deposita* 34, 505–521.

Breiter K., Frýda J. & Leichmann J. 2002: Phosphorus and rubidium in alkali feldspars: case studies and possible genetic interpretation. *Bull. Czech Geol. Survey* 77, 93–104.

Breiter K., Broska I. & Uher P. 2015: Intensive low-temperature tectono–hydrothermal overprint of peraluminous rare-metal granite: a case study from the Dlhá dolina Valley (Gemericum, Slovakia). *Geol. Carpath*. 66, 19–36.

Breiter K., Ďurišová J., Hrstka T., Hložková Vaňková M., Vašinová Galiová M., Kanický V., Rambousek P., Knésl I., Dobeš P. & Dosbaba M. 2017: Assessment of magmatic vs. metasomatic processes in rare metal granites: A case study of the Cínovec/Zinnwald Sn-W-Li deposit, Central Europe. *Lithos* 292–293, 198–201.

Broska I. & Uher P. 2001: Whole-rock chemistry and genetic typology of the West-Carpathian Variscan granites. *Geol. Carpath*. 52, 79–90.

Broska I., Uher P. & Lipka J. 1998: Brown and blue schorl from the Spiš–Gemer granite, Slovakia: composition and genetic relations. *J. Czech Geol. Soc*. 43, 9–16.

Broska I., Kubiš M., Williams C. & Konečný P. 2002: The compositions of rock-forming and accessory minerals from the Gemeric granites (Hnilec area, Gemeric Superunit, Western Carpathians). *Bull. Czech Geol. Survey* 77, 147–155.

Buriánek D. & Novák M. 2007: Compositional evolution and substitutions in disseminated and nodular tourmaline from leucocratic granites: examples from the Bohemian Massif, Czech Republic. *Lithos* 95, 148–164.

Cambel B., Kráľ J. & Burchart J. 1990: Isotopic geochronology of crystalline rock of the Western Carpathians. *Veda*, Bratislava, 1–183.

Chappell B.W. & White A.J.R. 2001: Two contrasting granite types: 25 years later. *Austrian J. Earth Sci.* 48, 489–499.

Charoy B., Chaussidon M., de Veslud L.C. & Duthou J.L. 2003: Evidence of Sr mobility in and around the albite-lepidolite-topaz granite of Beuvoir (France): an in situ ion and electron probe study of secondary Sr-rich phosphates. *Contrib Mineral. Petrol.* 145, 673–690.

Černý P. & Ercit T.S. 2005: The classification of granitic pegmatites revisited. *Can. Mineral.* 43, 2005–2026.

Dianiška I., Breiter K., Broska I., Kubiš M. & Malachovský P. 2002: First Phosphorus-rich Nb–Ta–Sn-specialised granite from the Carpathians Dlhá Dolina valey granite pluton, Gemeric Superunit, Slovakia. *Geol. Carpath.* 53, spec. iss., CD-ROM.

Dingwell D.B., Scarfe C.M. & Cronin D.J. 1985: The effect of fluorine on viscosities in the system Na_2O–Al_2O_3–SiO_2: implications for phonolites, trachytes and rhyolites. *Am. Mineral*. 70, 80–87.

Dingwell D.B., Pichavant M. & Holtz F. 1996: Experimental studies of boron in granitic melts. *Rev. Mineral. Geochem.* 33, 330–385.

Drivenes K., Larsen R.B., Müller A., Sorensen B.E., Wiedenbeck M. & Raanes M.P. 2015: Late-magmatic immiscibility during batholith formation: assessment of B isotopes and trace elements in tourmaline from the Land`s End granite, SW England. *Contrib. Mineral. Petrol.* 169, 56–83.

Duran C.J., Seydoux-Guillaume A.M., Bingen B., Gouy S., Parseval P., Ingrin J. & Guillaume D. 2016: Fluid-mediated alteration of (Y,REE,U,Th)-(Nb, Ta,Ti) oxide minerals in granitic pegmatite from the Evje-Iveland district, southern Norway. *Mineral. Petrol*. 110, 581–599.

Dutrow B.L. & Henry D.J. 2011: Tourmaline: a geologic DVD. *Elements* 7, 301–306.

Elliott B.A., O'Neill L.Ch. & Kyle J.R. 2017: Mineralogy and crystallisation history of highly differentiated REE-enriched hypabyssal rhyolite: Round Top laccolith Trans-Pecos, Texas. *Mineral. Petrol.* DOI 10.1007/s00710-017-0511-5

Faryad S. & Dianiška I. 1989: Garnets from granitoids of the Spišsko-gemerské Rudohorie Mts. *Geol. Zborn. Geol. Carpath*. 40, 715–734.

Finger F. & Broska I. 1999: The Gemeric S-type granites in southeastern Slovakia: late Palaeozoic or Alpine intrusions? Evidence from electron-microprobe dating of monazite. *Schweiz. Mineral. Petrogr. Mitt*. 79, 439–443.

Gaafar I.M. & Ali K.G. 2015: Geophysical and geochemical signature of rare metal granites, central eastern Desert, Egypt: Implications for tectonic environment. *Earth Sciences* 4, 5, 161–179.

Galliski M.A., Černý P., Márquez-Zavalia M.F. & Chapman R. 2012: An association of secondary Al–Li–Be–Ca–Sr phosphates in the San Elías pegmatite, San Luis, Argentina. *Can. Mineral.* 90, 933–942.

Grecula P., Abonyi A., Abonyiova M., Antaš J., Bartlaský B., Dianiška I., Drnzík E., Ďuďa R., Gargulák M., Gazdačko L., Macko J., Návesňák D., Németh Z., Novotný L., Radvanec M., Rojkovič I., Rozložník L., Rozložník O., Varček C. & Zlocha J. 1995: Mineral deposits of the Slovak Ore Mountains, volume 1. *Geocomplex*, Bratislava, 1–834.

Grecula P., Radvanec M. & Németh Z. 2000: Magnesite and talc mineralization in Slovakia. *Mineralia Slovaca* 32, 533–542.

Haapala I. 1997: Magmatic and postmagmatic processes in tin-bearing granites: topaz-bearing leucogranites in the Eurojoki rapakivi granite stock, Finland. *J. Petrol*. 38, 1645–1659.

Henry D.J., Novák M., Hawthorne F.C., Ertl A., Dutrow B.L., Uher P. & Pezzotta F. 2011: Nomenclature of the tourmaline-supergroup minerals. *Am. Mineral.* 96, 895–913.

Irber W. 1999: The lanthanide tetrad effect and its correlation with K/Rb, Eu/Eu*, Sr/Eu, Y/Ho, and Zr/Hf of evolving peraluminous granite suites. *Geochim. Cosmochim. Acta,* 63, 489–508.

Jiang S.Y., Radvanec M., Nakamura M., Palmer M., Kobayashi K., Zhao H.X. & Kui D.Z. 2008: Chemical and boron isotopic variations of tourmaline in the Hnilec granite-related hydrothermal system, Slovakia: Constrains on magmatic and metamorphic fluid evolution. *Lithos* 106, 1–11.

Jakabská K. & Rozložník L. 1989: Zircons of gemeric granites (Western Carpathians, Czechoslovakia). *Geol. Zborn. Geol. Carpath*. 40, 141–159.

Kamenický J. & Kamenický L. 1955: Gemeric granites and ore mineralisation of Spiš–Gemer Ore Mountains. *Geol Práce Zošit* 47, 1–73 (in Slovak).

Kohút M. & Reccio C. 2002: Sulphur isotope study of selected Hercynian granitic and surrounding rocks from the Western Carpathians (Slovakia). *Geol. Carpath*. 53, 3–13.

Kohút M. & Stein H. 2005: Re–Os molybdenite dating of granite-related Sn–W–Mo mineralisation at Hnilec, Gemeric Superunit, Slovakia. *Mineral. Petrol*. 85, 117–129.

Kohút M., Kovách V.P., Kotov A.B., Salnikova E.B. & Savatenkov V.M. 1999: Sr and Nd isotope geochemistry of hercynian granitic rocks from the Western Carpathians implications for granite genesis and crustal evolution. *Geol. Carpath*. 50, 477–487.

Kovách A., Svingor E. & Grecula P. 1986: Rb–Sr isotopic ages of granitoids from the Spišsko Gemerské Rudohorie Mts. *Mineralia Slovaca* 18, 1–14.

Krist E., Korikovskij S.P., Putiš M., Janák M. & Faryad S.W. 1992: Geology and petrology of metamoprhic rocks of the Western Carpathian crystalline complex. *Comenius University Press* Bratislava, 1–324.

Kubiš M. & Broska I. 2005: The role of boron and fluorine in evolved granitic rock system (on the example of the Hnilec area, Western Carpathians). *Geol. Carpath*. 56, 193–204.

Kubiš M. & Broska I. 2010: The granite system near Betliar village (Gemeric Superunit, Western Carpathians): evolution of a composite silicic reservoir. *J. Geosci*. 55, 131–148.

London D., Černý P., Loomis J.L. & Pan J.J. 1990: Phosphorus in alkali feldspars of rare-metal granitic pegmatites. *Can. Mineral.* 28, 771–786.

Lee S-G., Ahn I., Asahara Y., Tanaka T. & Lee S.R. 2018: Geochemical interpretation of magnesium and oxygen isotopic systematics in granites with the REE tetrad effect. *Geosci. J.* 22, 697–710.

Lexa O., Schulmann K.& Ježek J. 2003: Cretaceous collision and indentation in the West Carpathians: View based on structural analysis and numerical modeling. *Tectonics* 22, 6, 1066, doi:10.1029/2002TC001472.

Lukkari S., Thomas R. & Haapala I. 2009: Crystallization of the Kymi topaz granite stock within the Wiborg Rapakivi granite batholith, Finland: evidence from melt inclusions. *Can. Mineral.* 47, 1359–1374.

Malachovský P., Dianiška I., Matula I., Kamenický J., Kobulský J., Hodermarský J., Fabian M., Radvanec M., Kozáč J., Vlasák M., Mihalič A., Ščerbáková A., Seliga J. & Novoveský M. 1983: SGR — high temperature mineralization — Sn, W, Mo ores. *Open file report, Geofond*, Bratislava, 1–248 (in Slovak).

Malachovský P., Turanová L. & Dianiška I. 1992: Final report on mineral exploration from Gemerská Poloma. *Open file report, Geofond*, Bratislava, 1–180 (in Slovak).

Malachovský P., Uher P. & Ďuďa R. 2000: Nb-W minerals in rare metal granites, Dlhá dolina Spišsko Gemerské Rudohorie Mts. *Natura Carpatica* 41, 7–14 (in Slovak).

Manning D.A.C. 1981: The efekt of fluorine on liquidus phase relationship in the system Qz-Ab-Or with excess water at 1 kbar. *Contrib. Mineral. Petrol*. 76, 206–215.

Melcher F., Graupner T., Gäbler H-E., Sitnikova M., Oberthür T., Gerdes A., Badanina E. & Chudy T. 2017: Mineralogical and chemical evolution of tantalum-(niobium-tin) mineralisation in pegmatites and granites. Part 2: Worldwide examples (exluding Africa) and an overview of global mettalogenetic patterns. *Ore Geol. Rev.* 89, 946–987.

Müller A., Breiter K., Seltmann R. & Pécskay Z. 2005: Quartz and feldspar zoning in the eastern Erzgebirge volcano-plutonic complex (Germany, Czech Republic): evidence of multiple magma mixing. *Lithos* 80, 201–227.

Németh Z. 2002: Variscan suture zone in Gemericum: Contribution to reconstruction of geodynamic evolution and metallogenetic events of Inner Western Carpathians. *Slovak Geological Magazine* 8, 3–4, 247–257.

Pecho J., Beňka J., Gargulák M. & Václav J. 1980: Final report. Geological investigation of Sb deposits, Betliar–Čučma–Volovec area. *Open file report, Geofond*, Bratislava, 1–427 (in Slovak).

Perugini D. & Poli G. 2007: Tourmaline nodules from Capo Bianco aplite (Elba Island, Italy): an example of diffusion limited aggregation growth in a magmatic system. *Contrib. Mineral. Petrol.* 153, 493–508.

Petrasová K., Faryad S.H., Jeřábek P. & Žáčková E. 2007: Origin and metamorphic evolution of the magnesite–talc and adjacent rocks near Gemerská Poloma, Slovak Republic. *J. Geosci.* 52, 125–132.

Petrík I., Kubiš M., Konečný P., Broska I. & Malachovský P. 2011: Rare phosphates from the Surovec topaz–Li mica microgranite, Gemeric Unit, Western Carpathians, Slovak Republic: role of F/H_2O of the melt. *Can. Mineral*. 49, 521–540.

Petrík I., Čík Š., Miglierini M., Vaculovič T., Dianiška I. & Ozdín D. 2014: Alpine oxidation of lithium micas in Permian S-type granites (Gemeric unit, Western Carpathians, Slovakia). *Mineral. Mag*. 78, 507–533.

Pichavant M. 1981: An experimental study of the effect of boron on a water-saturated haplogranite at 1 kbar pressure. Geological applications. *Contrib. Mineral. Petrol.* 76, 430–439.

Plančár J., Fillo M., Šefara J., Snopko L. & Klinec A. 1977: Geophysical and geological interpretations of ore deposits and magnetic anomalies in Slovak Ore Mountains. *Západné Karpaty Geologia* 2, 7–114 (in Slovak with English summary).

Pollard P.J., Pichavant M. & Charoy B. 1987: Contrasting evolutin of fluorine- and boron-rich tin systems. *Miner. Deposita* 22, 315–321.

Poller U., Uher P., Broska I., Plašienka D. & Janák M. 2002: First Permian–Early Triassic ages for tin-bearing granites from the Gemeric unit (Western Carpathians, Slovakia): connection to the post-collisional extension of the Variscan orogen and S-type granite magmatism. *Terra Nova* 14, 41–48.

Pupin J.P. 1980: Zircon and granite petrology. *Contrib. Mineral. Petrol*. 73, 207–220.

Radvanec M. & Grecula P. 2016: Geotectonic and metallogenetic evolution of Gemericum (Inner Western Carpathians) from Ordovician to Jurassic. *Mineralia Slovaca* 48, 105–118.

Radvanec M., Koděra P. & Procháska W. 2004: Mg replacement at the Gemerska Poloma talc-magnesite deposit, Western Carpathians, Slovakia. *Acta Petrol. Sinica* 20, 773–790.

Radvanec M., Konečný P., Ondrejka M., Putiš M., Uher P. & Németh Z. 2009: The Gemeric granites as an indicator of the crustal extension above the Late-Variscan subduction zone and during the Early Alpine riftogenesis (Western Carpathians): an interpretation from the monazite and zircon ages dated by CHIME and SHRIMP methods. *Mineralia Slovaca* 41, 381–394 (in Slovak with English summary).

Roda-Robles E., Pesquera S., Gil P.P., Torres-Ruiz J. & Fontan F. 2004: Tourmaline from the rare-metal Pinilla pegmatite (Central Iberian zone, Zamora, Spain): chemical variation and implication for granite evolution. *Mineral. Petrol*. 81, 249–263.

Rojkovič I., Konečný P., Novotný L., Puškelová Ľ. & Streško V. 1999: Quartz–apatite–REE vein mineralisation in early palaeozoic rocks of the Gemeric superunit, Slovakia. *Geol. Carpath*. 50, 215–227.

Romer R.I. & Kroner U. 2016: Phanerozoic tin and tungsten mineralization — tectonic controls on the distribution of enriched protoliths and heat sources for crustal melting. *Gondwana Res*. 31, 60–95.

Rub M.G., Pavlov V.A., Cambel B. & Veselský J. 1977: Typomorphic properties of biotite and accessory minerals in the Gemeric granites of Slovakia. *Geol. Zbor. Geol. Carpath*. 28, 29–310 (in Russian).

Samson I.M. & Sinclair W.D. 1992: Magmatic hydrothermal fluids and the origin of quartz-tourmaline orbicles in the Seagull Batholith, Yukon Territory. *Can. Mineral*. 30, 937–954.

Simons B., Andersen J.C.O., Shail R.B. & Jenner F.E. 2017: Fractionation of Li, Be, Ga, Nb, Ta, In, Sn, Sb, W and Bi in the peraluminous Early Permian Variscan granites of the Cornubian Batholith: Precursor processes to magmatic-hydrothermal mineralisation. *Lithos* 278–281, 491–512.

Šefara J., Bielik M., Vozár J., Katona M., Szalaiová V. & Vozárová A. 2017: 3D density modelling of Gemeric granites of the Western Carpathians. *Geol. Carpath*. 68, 177–192.

Ševko M., Uher P., Sejkora J., Malíková R., Škoda R. & Vaculovič T. 2015: Phosphate minerals from the hydrothermal quartz veins in specialised S-type granites, Gemerská Poloma (Western Carpathians, Slovakia). *J. Geosci*. 60, 237–249.

Trumbull R.B., Krienitz M.S., Gottesmann B. & Wiedenbeck M. 2008: Chemical and boron-isotope variations in tourmalines from an S-type granite and its source rocks: the Erongo granite and tourmalinites in the Damara Belt, Nanibia. *Contrib. Mineral. Petrol.* 155, 1–18.

Uher P. & Broska I. 1996: Post-orogenic Permian granitic rocks in the Western Carpathian-Panonian area: geochemistry, mineralogy and evolution. *Geol. Carpath*. 47, 113–121.

Uher P., Malachovský P., Dianiška I. & Kubiš M. 2001: Rare-metal Nb–Ta–W mineralisation of the tin-bearing Spiš–Gemer granites, Eastern Slovakia. *Geolines* 13, 119–120.

van Hinsberg V.J., Henry D.J. & Marschall H.R. 2011: Tourmaline: an ideal indicator of its host environment. *Can. Mineral*. 49, 1–16.

Vozár J., Spišiak J., Vozárová A., Bazarnik J. & Kráľ J. 2015: Geochemistry and Sr, Nd isotopic composition of the Hronic Upper Paleozoic basic rocks (Western Carpathians, Slovakia). *Geol. Carpath*. 66, 3–17.

Yavuz F., Fuchs Y., Karakaya N. & Karakaya M.C. 2008: Chemical composition of tourmaline from the Asarck Pb Zn–Cu±U deposit, Şebinkarahisar, Turkey. *Mineral. Petrol*. 94, 195–208.

Appendix

Sample description and GPS location

Sample	Rock type, location	Longitude (°E)	Latitude (°N)	Altitude (m)
GK-6	porphyritic biotite granite, natural outcrop, Betliar	48°43’55.62”	20°31’47.71”	525
GK-7	rare metal granite, natural outcrop, Betliar	48°44’17.55”	20°31’48.89”	609
GK-8	medium grained, tourmaline granite, ore dump, Hnilec	48°49’35.11”	20°29’15.24”	720
GK-9	fine to medium grained muscovite granite, ore dump, Hnilec	48°49’35.11”	20°29’15.24”	720
GK-10	greisen, ore dump, Hnilec	48°49’35.11”	20°29’15.24”	720
GK-17	rare metal granite, natural outcrop, Betliar	48°44’18.87”	20°31’46.86”	640
GZ-1	medium grained, tourmaline granite, natural outcrop, Hnilec	48°48’54.88”	20°30’46.54”	726
GZ-12	aplite, natural outcrop, Poproč	48°43’26.01”	21°02’54.96”	489
ZK-31	muscovite granite, ore dump, Čučma	48°42’57.89”	20°33’27.24”	556
DD3-577	rare metal granite, drill core DD-3; depth 577 m, Dlhá dolina	48°45’56.63”	20°32’07.49”	801
DD3-594	rare metal granite, drill core DD-3; depth 594 m, Dlhá dolina	48°45’56.63”	20°32’07.49”	801
DD3-908	porphyritic biotite granite, drill core DD-3; depth 908 m, Dlhá dolina	48°45’56.63”	20°32’07.49”	801
LIG-17	topaz–Li mica microgranite, taken from trench, Surovec (see Petrík et al. 2011)	48°47’33.04”	20°33’40.69”	766